Epitranscriptomic N^6-methyladenosine profile of SARS-CoV-2-infected human lung epithelial cells

Stacia Phillips, Shaubhagya Khadka, Dana Bohan, Constanza E. Espada, Wendy Maury, Li Wu*

Department of Microbiology and Immunology, Carver College of Medicine, University of Iowa, Iowa City, IA, 52240, USA

* Corresponding author. Li Wu. Email address: li-wu@uiowa.edu

Keywords: SARS-CoV-2, epitranscriptomics, N^6-methyladenosine, microarray, lung epithelial cells, infection

Abstract

N^6-methyladenosine (m^{6}A) is a dynamic post-transcriptional RNA modification that plays an important role in determining transcript fate. Severe acute respiratory syndrome-related coronavirus 2 (SARS-CoV-2) has caused the global pandemic of coronavirus disease 2019 (COVID-19) and the virus has been extensively studied. However, how m^{6}A modification of host cell RNAs change during SARS-CoV-2 infection has not been reported. Here we define the epitranscriptomic m^{6}A profile of SARS-CoV-2-infected human lung epithelial cells compared to uninfected controls. Biological pathway analyses revealed that differentially methylated transcripts were significantly associated with cancer-related pathways, protein processing in the endoplasmic reticulum, cell death and proliferation. Upstream regulators predicted to be associated with the proteins encoded by differentially methylated mRNAs include proteins involved in the type I interferon response, inflammation, and cytokine signaling. These data suggest that m^{6}A modification of cellular RNA is an important mechanism of regulating host gene expression during SARS-CoV-2 infection of lung epithelial cells.

Introduction

N^6-methyladenosine (m^{6}A) is the most prevalent post-transcriptional modification of eukaryotic mRNA and plays an important role in the fate the modified mRNA molecule. The m^{6}A is deposited on adenosine by a methyltransferase, or “writer”, complex consisting of the catalytic heterodimer methyltransferase-like-3 and methyltransferase-like14 (METTL3/METTL14) in complex with the adapter protein Wilms tumor 1-associated protein (WTAP) (Liu et al., 2014). m^{6}A is also prevalent on small non-coding RNA (sncRNA) and long non-coding RNA (lncRNA) and this modification is catalyzed by the writer METTL16 (Warda et al., 2017). Two demethylases, or “erasers”, fat mass and obesity-associated protein (FTO) and α-ketoglutarate-dependent

dioxygenase AlkB homolog 5 (ALKBH5) can remove the m^{6}A modification, suggesting that m^{6}A modification is not only dynamic but reversible (Jia et al., 2011; Zheng et al., 2013). The outcome of m^{6}A modification is dictated by m^{6}A-specific RNA binding proteins or "readers", the most well characterized of which are members of the YT521-B homology (YTH) family (Patil et al., 2018; Zaccara and Jaffrey, 2020). Binding of readers to the modified mRNA can lead to changes in stability, translation, localization, and splicing (Lesbirel and Wilson, 2019; Roundtree et al., 2017; Wang et al., 2014; Wang et al., 2015; Zhao et al., 2014; Zheng et al., 2017). Therefore, m^{6}A modification acts as an important mechanism of post-transcriptional regulation of gene expression.

Many virus genomes and viral RNAs are m^{6}A-modified, and these modifications play important functional roles in various stages of virus replication and evasion of innate immune sensing (Imam et al., 2020). SARS-CoV-2 RNAs are m^{6}A-modified and while some cell type-dependent discrepancies exist, most studies have reported that m^{6}A is required for efficient virus replication (Burgess et al., 2021; Campos et al., 2021; Li et al., 2021a; Liu et al., 2021; Zhang et al., 2021). In addition to functional m^{6}A modification of viral RNAs, changes in the cellular m^{6}A methylome have also been shown to occur in association with viral infections (Gokhale et al., 2020; McFadden and Horner, 2021; Williams et al., 2019). Of particular interest, cellular transcripts involved in establishing an antiviral immune response are post-transcriptionally regulated by m^{6}A modification (McFadden et al., 2021; Rubio et al., 2018; Winkler et al., 2019). It is likely that SARS-CoV-2 infection leads to changes in the m^{6}A modification state of host cell transcripts, either induced directly by the virus or through the cellular response to infection. Indeed, m^{6}A sequencing (m^{6}A-seq or meRIP-seq) has revealed the loss or gain of m^{6}A modifications in host cell RNA from infected cells (Liu et al., 2021). However, how the host m^{6}A methylome changes in human lung cells in response to SARS-CoV-2 infection remains unknown.

Here we report the results of epitranscriptomic m^{6}A microarray analysis of human lung cells infected with SARS-CoV-2 compared to uninfected control cells. We identified changes in the abundance of methylated cellular RNAs for both protein-coding and non-coding transcripts. One micro-RNA (miR) precursor, miR-4486, was found to be 175 times more abundant in the methylated fraction of infected-cell RNA compared to uninfected controls. Interestingly, biological pathway analysis revealed that many differentially methylated mRNA transcripts code for proteins that are regulated upstream by proteins involved in inflammation, cytokine signaling, and innate immunity. These findings will serve as the basis for future functional validation studies to determine how changes in the methylation status of host cell transcripts may affect SARS-CoV-2 replication and viral pathogenesis.

Results

A549-hACE2 cells support productive SARS-CoV-2 infection

We sought to determine the epitranscriptomic m^{6}A profile of SARS-CoV-2-infected cell RNA using a human lung epithelial cell line, as lung epithelial cells represent a biologically relevant target of SARS-CoV-2. Robust and reliable identification of changes to the methylation level of individual host cell transcripts during infection is best achieved using conditions under which most of the cells have become infected, reducing background signal contributed by uninfected cells. Therefore, we first directly compared three different lung cell lines (A549-hACE2 cells expressing human angiotensin-converting enzyme 2 [hACE2], Calu-3, and H1650) for their ability to support SARS-CoV-2 replication under identical conditions. In our infection assays, we chose to infect cells with SARS-CoV-2 (strain USA-WA-1/2020) at a multiplicity of infection (MOI) of 1 for 24 hours to allow for a full viral life cycle and spreading infection to occur (Li et al., 2021b). After 24 hours, A549-hACE2 cells were fixed, and infected cells were visualized by immunofluorescent

staining using a SARS-CoV-2 nucleocapsid-specific antibody (Fig. 1A). Infection of A549-hACE2 cells resulted in a greater proportion of N-positive cells (~70%) compared to Calu-3 and H1650 cell lines (data not shown). Real-Time quantitative PCR (RT-qPCR) analysis using *spike* gene-specific qPCR primers demonstrated robust viral RNA replication in A549-hACE2 cells with ~5 $\times$ 10^4 copies of spike RNA present per infected cell (Fig. 1B). These RNA molecules represent both full-length positive sense RNA and subgenomic RNA used for translation to viral protein. Based on these results, we chose to use A549-hACE2 cells to determine the epitranscriptomic m^6A profile of SARS-CoV-2-infected cells.

SARS-CoV-2 infection of A549-hACE2 cells leads to differential m^6A modification of cellular RNA

To analyze m^6A modifications of host cell transcripts, A549-hACE2 cells were infected with SARS-CoV-2 at an MOI of 1 for 24 hours in biological triplicate. Total RNA from SARS-CoV-2-infected cells and mock-infected negative control cells was used for m^6A immunoprecipitation (IP) followed by microarray analysis using the Arraystar Epitranscriptomic m^6A Array (see schematic method summary in Fig. 2A). The RNA present in the IP fraction represents m^6A-modified RNA, whereas the remaining unbound fraction is assumed to be unmethylated. Each fraction was fluorescently labeled and mixed prior to array hybridization. The microarray contains over 60,000 unique probes (60 nt each) that represent 44,122 mRNA, 12,496 lncRNA, 1,366 pre-miRNA, 1,642 pri-miRNA, 19 small nuclear RNA (snRNA), and 786 small nucleolar RNA (snoRNA) transcripts. Unique mRNA splice isoforms are distinguished by probes that are exon specific or span a splice junction. Signal for each transcript in the IP and unbound fractions was normalized to the intensity of non-human spike-in RNA.

Transcript types that were found to be significantly differentially methylated ≥ 1.5-fold with a p-value ≤ 0.05 in SARS-CoV-2-infected cells compared to mock-infected controls are summarized in Table 1. A total of 186 unique transcripts were hypomethylated and 119 transcripts were hypermethylated in response to infection. A volcano plot shows the statistical significance (-log10 p-value) versus the fold change (log2 FC) in the abundance of methylated transcript in SARS-CoV-2-infected cells relative to mock (Fig. 2B). A selection of transcripts with the most significant changes in m^6A abundance (p-value ≤ 0.005) are shown in Table 2. The full list of transcripts with significantly different m^6A abundance in infected cells can be found in Table S1 (p-value ≤ 0.05, fold change ≥ 1.5).

The plot of log2 FC shows that changes in hypomethylated transcripts ranged from a log2 FC of -0.59 to -1.52 (1.5-fold to 2.8-fold change). Similarly, the log2 FC for most transcripts found to be hypermethylated in infected cells ranged from 0.59 to 1.47 (1.5-fold to 2.8-fold change). Eight of the hypermethylated transcripts showed a greater than 3-fold change. Remarkably, the primary miR transcript for miR-4486 was found in the methylated RNA fraction from infected cells at a 175-fold higher level than in uninfected controls. The associated p-value of this change was 2.41×10^{-6}, demonstrating high reproducibility among three independent infections and uninfected controls (Fig. 2B and Table S1).

A unique feature of the epitranscriptomic microarray is the ability to determine the percentage of transcript molecules that are m^6A-modified, based on the relative intensity of signals in the IP and unbound fractions. This stoichiometric information is not provided by other m^6A detection techniques such as m^6A-seq (Dominissini et al., 2012; McIntyre et al., 2020). Selected transcripts with a significantly different percentage of m^6A-modified RNA in SARS-CoV-2-infected samples relative to mock controls are shown in Table 3 (p-value ≤ 0.005). The full list of transcripts with a significantly different percentage of m^6A-modified RNA in infected cells can be found in Table S1 (p-value ≤ 0.05). These results show that many cellular transcripts undergo

changes in m^6A abundance and percentage of transcript modified in response to SARS-CoV-2 infection of A549-hACE2 cells.

Biological pathway analysis of differentially methylated protein-coding transcripts

Protein coding transcripts were analyzed by iPathwayGuide (Advaita) to identify biological pathways that are significantly associated with cellular mRNAs that are differentially methylated in response to SARS-CoV-2 infection of A549-hACE2 cells. The p-values for significance of the association are derived from a combination of two independent analyses, classical over-representation analysis (pORA) and a measure of accumulated perturbation of a given pathway (pAcc) (Ahsan and Draghici, 2017; Donato et al., 2013; Draghici et al., 2007; Tarca et al., 2009). The full list of pathways associated with at least one differentially methylated mRNA is listed in Table S2, with pAcc, pORA, and the combined p-value indicated. Pathways with no pAcc represent metabolic networks, as opposed to signaling pathways which have both pAcc and pORA.

Fig. 3 shows the list of pathways with the highest combined significance ($p \leq 0.005$). We found that protein coding transcripts that are differentially methylated in response to SARS-CoV-2 infection are associated with several cancer-related pathways (microRNAs, pathways, proteoglycans, and programmed death ligand 1 [PD-L1] expression and PD-1 checkpoint pathways in cancer), infectious disease (Legionellosis, Kaposi sarcoma-associated herpesvirus infection, and Hepatitis B), cell metabolism, proliferation, and survival/death (protein processing in the endoplasmic reticulum, metabolic pathways, necroptosis, forkhead box O [FoxO] signaling, mitophagy, epidermal growth factor receptor [EGFR] tyrosine kinase inhibitor resistance, signaling pathways regulating pluripotency of stem cells, phosphoinositide-3-kinase-Akt [PI3K-Akt] signaling), and the immune response (JAK-STAT signaling). Our data also indicated the

number of differentially methylated transcripts that are associated with each pathway (count) and the -log10 of the associated combined p-value. Together, these results suggest complex and dynamic biological pathways are involved in cellular responses to SARS-CoV-2 infection.

Upstream regulators of differentially methylated mRNAs and predicated networks.

To further analyze the significant regulators of differentially methylated transcripts during SARS-CoV-2 infection, iPathwayGuide was also used to identify putative upstream regulators of proteins encoded for by transcripts found to be differentially methylated in SARS-CoV-2-infected cells compared to mock-infected control cells. Interestingly, the top 20 upstream regulators predicted with the highest significance ($p \leq 0.01$) were enriched for proteins involved in inflammation, cytokine signaling, and innate immunity (Fig. 4). The most significantly associated predicted upstream regulator is EGFR, which has been implicated as a potential therapeutic target for COVID-19 treatment (Klann et al., 2020; Londres et al., 2022; Vagapova et al., 2021; Venkataraman and Frieman, 2017). Other predicted upstream regulators with known function in inflammation and innate immunity include mitogen-activated protein kinase kinase 7 (MAP2K7), tumor necrosis factor receptor superfamily member 1A (TNFRSF1A), sprouty RTK signaling antagonist 4 (SPRY4), Janus kinase 3 (JAK3), Janus kinase 2 (JAK2), interferon alpha 1 (IFNA1), and tumor necrosis factor (TNF).

To better understand the interactions among significant regulators, predicted upstream regulators of differentially methylated transcripts were used to construct networks illustrating known regulatory interactions among individual nodes of a given pathway. Selected upstream regulators and their downstream targets that are differentially methylated in response to SARS-CoV-2 infection are indicated, with hypomethylated transcripts shown in blue and hypermethylated transcripts in pink (Fig. 5A-C). Gray nodes represent intermediate genes in the

pathway that directly regulate or are regulated by differentially methylated pathway members, but do not themselves exhibit any change in methylation status upon SARS-CoV-2 infection. Pink arrows illustrate activation and gray bars represent inhibition for functional interactions that have been experimentally validated (Fig. 5A-C). These analyses allow us to develop novel hypotheses regarding how the host cell responds to SARS-CoV-2 infection. Together, these results suggest that regulation of gene expression at the level of post-transcriptional RNA modification is a mechanism by which the cell responds to SARS-CoV-2 infection and may have effects on viral pathogenesis and the immune response.

Discussion

Post-transcriptional m^6A modification of RNA is an important strategy for regulation of gene expression (Shi et al., 2019). We sought to identify changes in m^6A modification of cellular RNA during SARS-CoV-2 infection of human lung epithelial cells using epitranscriptomic m^6A microarray analysis. These cellular RNAs may be important for virus replication or for establishing an antiviral innate immune response. We identified mRNA and long and small non-coding RNA species that are differentially m^6A-modified in response to SARS-CoV-2 infection. Differentially methylated mRNA transcripts were found to be associated with biological pathways and upstream regulators that are involved in the immune response to viral infection. These data may provide a basis for novel hypotheses regarding mechanisms of SARS-CoV-2 replication or the cellular response to infection of lung epithelial cells. Future functional studies of the identified cellular RNA are required to test these hypotheses.

Overall, we observed differential methylation of 305 unique transcripts, with 186 hypomethylated and 119 hypermethylated transcripts in infected cells compared to uninfected controls. These differentially methylated transcripts are a relatively small percentage of all

transcripts represented on the epitranscriptomic microarray (Table 1). The number of transcripts and magnitude of differential methylation in the current study is likely an underestimation of the actual change in methylation status that occurs in infected cells, due to the contribution of RNA from the ~30% of cells in infected cultures that remained uninfected when the RNA was harvested (Fig. 1A). Some effects may also be missed due to differences in IP efficiency of individual transcripts, due either to RNA length or location of the m^6A modification(s). Although the consensus RRACH motif (R = A or G; H = A, C, or U) for m^6A modification is relatively common, only ~5% of these motifs are m^6A modified, resulting in an average of 1-2 m^6A modifications per mRNA transcript (Dominissini et al., 2012). Therefore, despite the limitations described above, it is possible that modest changes in m^6A modification can potentiate changes to RNA function during SARS-CoV-2 infection.

One mRNA found to be significantly more m^6A-modified in infected cells compared to mock-infected controls is the muscle-associated receptor tyrosine kinase (MUSK). The epitranscriptomic microarray indicated that this mRNA is present at ~8-fold greater abundance in the m^6A-IP fraction in infected cells and that the percentage of methylated transcript increased from 30% in uninfected cells to 69% in SARS-CoV-2-infected cells (Tables 2 and 3). MUSK is a receptor tyrosine kinase that is essential for the formation and maintenance of the neuromuscular junction and is expressed at very low levels in the lung under normal conditions (Uhlen et al., 2015). Auto-antibodies directed against MUSK inhibit acetylcholine receptor clustering at the neuromuscular junction and are associated with a rare form of myasthenia gravis (MG), a chronic autoimmune disorder in which antibodies destroy the communication between nerves and muscle, resulting in weakness of the skeletal muscles (Hoch et al., 2001). Interestingly, a recent case report identified the development of MUSK-associated MG potentially triggered by SARS-CoV-2 infection (Assini et al., 2021). It would be important to investigate how SARS-CoV-2

229 infection could induce the development of autoantibodies to MUSK or how this might involve post-
230 transcriptional m^{6}A modifications of the MUSK mRNA.

231 We also observed a modest but significant increase in the levels of m^{6}A modification of
232 signal transducer and activator of transcription-3 (STAT3) transcript (Table 3). This transcription
233 factor plays a pivotal role in intracellular signaling and subsequent activation of gene expression
234 in response to a variety of cytokines and chemokines, including IL-6 and type I interferons
235 (Villarino et al., 2017). STAT3 may contribute to the pathogenesis of SARS-CoV-2 infection in a
236 variety of ways considering its pleiotropic effects on inflammation and the immune response
237 [reviewed in (Jafarzadeh et al., 2021)]. We also observed changes in the abundance of m^{6}A-
238 modified JAK1 and STAT6 transcripts, which are also part of the JAK/STAT signaling pathway
239 and may functionally interact with each other as part of the host cell response to infection (Table
240 S1 and Fig. 5C). Consistent with these results, pathway analysis revealed that the JAK-STAT
241 pathway was significantly associated with differentially methylated mRNAs in infected cells (Fig.
242 3). Therefore, other members of the JAK-STAT pathway were identified as upstream regulators
243 of the protein products of mRNAs found to be differentially methylated in infected cells (Fig. 4,
244 Fig. 5A and 5C). This overrepresentation of the JAK-STAT pathway in our analyses may reflect
245 the activation of the JAK-STAT pathway in both bystander and infected cells.

246 The cellular RNA found to be the most significantly differentially methylated in response
247 to SARS-CoV-2 infection was the precursor of miR-4486 (Tables 2 and 3, and Fig. 2B). Due to
248 the size of the microarray probes (60 nt), miR transcripts are represented by the unprocessed
249 primary and precursor transcripts, which may serve as a proxy for the mature 22 nt functional
250 miR. One functionally validated target of miR-4486 is JAK3, which was also identified in our
251 analysis as an upstream regulator significantly associated with differentially methylated
252 transcripts in SARS-CoV-2-infected cells (Figs. 4 and 5C) (Zhou et al., 2022). One possible
253 hypothesis based on our network analysis is that degradation of JAK3 transcript by miR-4486

leads to lower STAT3 activation as a compensatory mechanism in the infected cell to counteract SARS-CoV-2-induced STAT3 hyperactivation (Fig. 5C) (Matsuyama et al., 2020). The cellular lncRNA SNHG20 acts as a competing endogenous RNA to sponge miR-4486 and prevent degradation of miR-4486 target transcripts (Liu et al., 2019; Liu et al., 2022). Interestingly, a meta-analysis of transcriptomic data sets from COVID-19 patient samples found that SNHG20 was among the top 10 most significantly upregulated lncRNAs (Chakraborty et al., 2021). It is possible that miR-4486 is upregulated early in infected cells, whereas SNHG20 is upregulated at later times to counteract inhibition of cellular gene expression by miR-4486. Finally, experimentally validated binding targets of miR-4486 include TNF receptor-associated factor 7 (TRAF7) (Karginov and Hannon, 2013) and interleukin 1 receptor-associated kinase 3 (IRAK3) (Karginov and Hannon, 2013), both of which are involved in innate immune signaling and can lead to inhibition of NF-κB activation (Kobayashi et al., 2002; Zotti et al., 2012). Further studies are needed to determine which of these miR-4486 targets are functionally relevant during SARS-CoV-2 infection of human lung epithelial cells.

EGFR was identified as the putative upstream regulator predicted to be associated with differentially methylated mRNA transcripts with the highest confidence (Fig. 4). A network map illustrates the potential functional interactions between EGFR and proteins downstream whose mRNA were found to be hypermethylated (RAS p21 protein activator 1 [RASA1] and STAT3) and hypomethylated (hypoxia inducible factor 1 [HIF1A] and BCL2 like 11 [BCL2L11]). Several studies have demonstrated that EGFR is highly expressed and that EGFR signaling activity contributes to lung fibrosis in COVID-19 patients, leading to the identification of EGFR as a potential therapeutic target for treating severe COVID-19 (Klann et al., 2020; Londres et al., 2022; Vagapova et al., 2021).

The effect of reversible and dynamic m^6A modification on a given transcript is context dependent and may be inhibitory (destabilization or sequestration) or activating (enhanced

translation or splicing) (Lesbirel and Wilson, 2019; Roundtree et al., 2017; Wang et al., 2014; Wang et al., 2015; Zhao et al., 2014; Zheng et al., 2017). Networks such as those shown in Fig. 5 are useful for predicting functional associations between differentially methylated transcripts and identifying other members of a given signaling pathway that may also be affected by the change in m^6A modification. However, due to potential opposing functional effects of m^6A modification on an mRNA, it may not be straightforward to predict the directionality of effect on a downstream pathway member caused by changes in methylation of an upstream mRNA target.

In summary, our analysis identifies many cellular RNAs that exhibit differential methylation in SARS-CoV-2-infected human lung epithelial cells. These results can lay the foundation for the broader research community for the formation of novel hypotheses regarding the role of post-transcriptional regulation of host gene expression during SARS-CoV-2 infection. Our future studies are focused on functional validation of selected transcripts and determining the biological significance of differential methylation of specific transcripts during SARS-CoV-2 infection of primary human airway epithelia cells.

Material and methods

Cells and SARS-CoV-2 infection. A549-hACE2 lung carcinoma cells expressing the human ACE2 protein (Invivogen) were maintained in DMEM with 4.5 g/L glucose and 2 mM L-glutamine (Gibco), 10% heat-inactivated fetal bovine serum (FBS, R&D Systems), 100 U/mL penicillin, 100 µg/mL streptomycin (Gibco), and 0.5 µg/mL puromycin (Sigma). Vero E6 TMPRSS2 cells were maintained in DMEM with 4.5 g/L glucose and 2 mM L-glutamine (Gibco), 10% heat-inactivated FBS (R&D Systems), 100 U/mL penicillin and 100 µg/mL streptomycin (Gibco), and 5 µg/mL blasticidin (Invivogen). SARS-CoV-2 strain 2019n-CoV/USA-WA-1/2020 (BEI, Cat. #NR-52281) was propagated on Vero TMPRSS2 cells as described (Bohan et al., 2021). Infected cell

supernatant containing virus was collected, passed through a 0.45 µM filter, and concentrated by centrifugation at 10,000 × g for 24 hours at 10°C. Virus titer was determined by $TCID_{50}$ assay on Vero TMPRSS2 cells (Bohan et al., 2021).

Immunofluorescence. At 24 hours post-infection, A549-hACE2 cells were fixed with 4% PFA (Electron Microscopy Sciences, Cat. #15710) for 30 min at room temperature and permeabilized with 0.5% Triton X-100 in phosphate buffered saline. Cells were incubated with rabbit monoclonal SARS-CoV/SARS-CoV-2 nucleocapsid antibody (SinoBiological 40143-R001, dilution 1:100), followed by incubation with Alexa Fluor 488 goat anti-rabbit IgG (Life Technologies, dilution 1:500). Nuclei are stained with DAPI (1 µg/ml). Images were acquired with a Nikon Eclipse Ts2 microscope.

RT-qPCR. Total cellular RNA was purified using TRIzol reagent according to the manufacturer's protocol (Invitrogen). RNA concentration was determined using a Nanodrop-OneC spectrophotometer (Thermo Fisher). RNA was DNase-treated using TURBO DNase according to the manufacturer's protocol (Thermo). 100 ng DNase-treated RNA was used as template for cDNA synthesis using the iScript cDNA Synthesis Kit according to the manufacturer's protocol (Bio-Rad). The resulting cDNA was diluted 1:10 and 2 µL was used for qPCR amplification of SARS-CoV-2 spike using iTaq Universal SYBR Green Supermix according to the manufacturer's protocol (Bio-Rad). Copy number was calculated in reference to a standard curve of known copy number (10^2 – 10^7 copies spike). The following two primers were used at a final concentration of 200 nM (Bohan et al., 2021):

SARS-CoV-2 S forward: 5' - CTACATGCACCAGCAACTGT – 3'

SARS-CoV-2 S reverse: 5' - CACCTGTGCCTGTTAAACCA – 3'

m^{6}A immunoprecipitation. Total cellular RNA was purified using TRIzol reagent according to the manufacturer's protocol (Invitrogen). RNA concentration was determined using a Nanodrop-OneC spectrophotometer (Thermo Fisher). 5 μg total RNA and m^{6}A spike-in control mixture were added to 300 μL 1× IP buffer (50 mM Tris-HCl, pH 7.4, 150 mM NaCl, 0.1% NP40, 40U/μL RNase Inhibitor) containing 2 μg anti-m^{6}A rabbit polyclonal antibody (Synaptic Systems). The reaction was incubated with head-over-tail rotation at 4°C for 2 hours. 20 μL Dynabeads™ M-280 Sheep Anti-Rabbit IgG suspension per sample was blocked with freshly prepared 0.5% BSA at 4°C for 2 hours, washed three times with 300 μL 1× IP buffer, and resuspended in the total RNA-antibody mixture prepared above. The RNA binding to the m^{6}A-antibody beads was carried out with head-over-tail rotation at 4°C for 2 hours. The beads were then washed three times with 500 μL 1× IP buffer and twice with 500 μL Wash buffer (50 mM Tris-HCl, pH 7.4, 50 mM NaCl, 0.1% NP40, 40 U/μL RNase Inhibitor). The enriched RNA was eluted with 200 μL Elution buffer (10 mM Tris-HCl, pH 7.4, 1 mM EDTA, 0.05% SDS, 40U Proteinase K, 1 μL RNase inhibitor) at 50°C for 1 hour. The RNA was extracted by acid phenol-chloroform and ethanol precipitated.

RNA labeling and hybridization. The immunoprecipitated (IP) RNAs and unbound RNAs were mixed with equal amount of calibration spike-in control RNA, separately amplified and labeled with Cy3 (unbound) and Cy5 (IP) using Arraystar Super RNA Labeling Kit. The synthesized cRNAs were purified by RNeasy Mini Kit (Qiagen). The concentration and specific activity (pmol dye/μg cRNA) were measured with NanoDrop ND-1000. Cy3 and Cy5 labeled cRNAs were mixed and 2.5 μg of the cRNA mixture in 19 μL volume was fragmented by adding 5 μL 10× Blocking Agent and 1 μL of 25× Fragmentation Buffer, followed by heating at 60°C for 30 min. The fragmented RNA was combined with 25 μL 2× Hybridization buffer. 50 μL hybridization solution

was dispensed into the gasket slide and assembled to the m^{6}A-mRNA&lncRNA Epitranscriptomic Microarray slide. The slides were incubated at 65°C for 17 hours in an Agilent Hybridization Oven. The hybridized arrays were washed, fixed, and scanned using an Agilent Scanner (G2505C).

Data and statistical analysis. Agilent Feature Extraction software (version 11.0.1.1) was used to analyze acquired array images. Raw intensities of IP (Cy5-labelled) and unbound (Cy3-labelled) were normalized using the average of log2-scaled Spike-in RNA intensities. After Spike-in normalization, the probe signals having present or marginal QC flags in at least 3 out of 6 samples were retained for further "m^{6}A quantity" analyses. "m^{6}A quantity" was calculated for the m^{6}A methylation amount based on the IP (Cy5-labelled) normalized intensities. Differentially m^{6}A-methylated RNAs between two comparison groups were identified by filtering with the fold change and statistical significance (p-value) thresholds. Protein-coding transcripts that were found to be differentially m^{6}A-methylated between mock and SARS-CoV-2-infected samples with a fold change ≥1.5 and a p-value ≤0.05 were uploaded to iPathwayGuide (ipathwayguide.advaitabio.com) for gene ontology, pathway, upstream regulator, and network analyses (Ahsan and Draghici, 2017; Donato et al., 2013; Draghici et al., 2007; Tarca et al., 2009).

Funding

This work was supported by the National Institutes of Health grant R21AI159546 to L.W. The funder had no role in study design, data collection and analysis, decision to publish, or preparation of the manuscript.

CRediT authorship contribution statement

374 **Stacia Phillips:** Conceptualization, Methodology, Formal analysis, Investigation, Writing –
375 Original Draft, Writing – Review & Editing, Visualization, Supervision, Project administration.
376 **Shaubhagya Khadka:** Investigation. **Dana Bohan:** Investigation, Writing – Review & Editing.
377 **Constanza Espada:** Investigation, Writing – Review & Editing. **Wendy Maury:** Methodology,
378 Resources, Writing – Review & Editing, Supervision. **Li Wu:** Conceptualization, Methodology,
379 Writing – Review & Editing, Visualization, Supervision, Project administration, Funding
380 acquisition.

381

382 **Declaration of competing interest**

383 The authors declare that they have no known competing financial interests or personal
384 relationships that could have appeared to influence the work reported in this paper.

385

386 **Acknowledgments**

387 The following reagent was deposited by the Centers for Disease Control and Prevention and
388 obtained through BEI Resources, NIAID, NIH: SARS-Related Coronavirus 2, Isolate USA-
389 WA1/2020, NR-52281. We thank Dr. Michael Chimenti for helpful discussion and assistance with
390 iPathway Guide analysis. We thank Dr. Patrick Sinn for A549-hACE2 cells.

391

392 **References**

393 Ahsan, S., Draghici, S., 2017. Identifying Significantly Impacted Pathways and Putative
394 Mechanisms with iPathwayGuide. Curr Protoc Bioinformatics 57, 7 15 11-17 15 30.

395 Assini, A., Gandoglia, I., Damato, V., Rikani, K., Evoli, A., Del Sette, M., 2021. Myasthenia gravis
396 associated with anti-MuSK antibodies developed after SARS-CoV-2 infection. Eur J Neurol 28,
397 3537-3539.

Bohan, D., Van Ert, H., Ruggio, N., Rogers, K.J., Badreddine, M., Aguilar Briseno, J.A., Elliff, J.M., Rojas Chavez, R.A., Gao, B., Stokowy, T., Christakou, E., Kursula, P., Micklem, D., Gausdal, G., Haim, H., Minna, J., Lorens, J.B., Maury, W., 2021. Phosphatidylserine receptors enhance SARS-CoV-2 infection. PLoS Pathog 17, e1009743.

Burgess, H.M., Depledge, D.P., Thompson, L., Srinivas, K.P., Grande, R.C., Vink, E.I., Abebe, J.S., Blackaby, W.P., Hendrick, A., Albertella, M.R., Kouzarides, T., Stapleford, K.A., Wilson, A.C., Mohr, I., 2021. Targeting the m(6)A RNA modification pathway blocks SARS-CoV-2 and HCoV-OC43 replication. Genes Dev 35, 1005-1019.

Campos, J.H.C., Maricato, J.T., Braconi, C.T., Antoneli, F., Janini, L.M.R., Briones, M.R.S., 2021. Direct RNA Sequencing Reveals SARS-CoV-2 m6A Sites and Possible Differential DRACH Motif Methylation among Variants. Viruses 13.

Chakraborty, C., Sharma, A.R., Bhattacharya, M., Zayed, H., Lee, S.S., 2021. Understanding Gene Expression and Transcriptome Profiling of COVID-19: An Initiative Towards the Mapping of Protective Immunity Genes Against SARS-CoV-2 Infection. Front Immunol 12, 724936.

Dominissini, D., Moshitch-Moshkovitz, S., Schwartz, S., Salmon-Divon, M., Ungar, L., Osenberg, S., Cesarkas, K., Jacob-Hirsch, J., Amariglio, N., Kupiec, M., Sorek, R., Rechavi, G., 2012. Topology of the human and mouse m6A RNA methylomes revealed by m6A-seq. Nature 485, 201-206.

Donato, M., Xu, Z., Tomoiaga, A., Granneman, J.G., Mackenzie, R.G., Bao, R., Than, N.G., Westfall, P.H., Romero, R., Draghici, S., 2013. Analysis and correction of crosstalk effects in pathway analysis. Genome Res 23, 1885-1893.

Draghici, S., Khatri, P., Tarca, A.L., Amin, K., Done, A., Voichita, C., Georgescu, C., Romero, R., 2007. A systems biology approach for pathway level analysis. Genome Res 17, 1537-1545.

Gokhale, N.S., McIntyre, A.B.R., Mattocks, M.D., Holley, C.L., Lazear, H.M., Mason, C.E., Horner, S.M., 2020. Altered m(6)A Modification of Specific Cellular Transcripts Affects Flaviviridae Infection. Molecular cell 77, 542-555 e548.

Hoch, W., McConville, J., Helms, S., Newsom-Davis, J., Melms, A., Vincent, A., 2001. Auto-antibodies to the receptor tyrosine kinase MuSK in patients with myasthenia gravis without acetylcholine receptor antibodies. Nat Med 7, 365-368.

Imam, H., Kim, G.W., Siddiqui, A., 2020. Epitranscriptomic(N6-methyladenosine) Modification of Viral RNA and Virus-Host Interactions. Front Cell Infect Microbiol 10, 584283.

429 Jafarzadeh, A., Nemati, M., Jafarzadeh, S., 2021. Contribution of STAT3 to the pathogenesis of
430 COVID-19. Microb Pathog 154, 104836.

431 Jia, G., Fu, Y., Zhao, X., Dai, Q., Zheng, G., Yang, Y., Yi, C., Lindahl, T., Pan, T., Yang, Y.G., He,
432 C., 2011. N6-methyladenosine in nuclear RNA is a major substrate of the obesity-associated FTO.
433 Nat Chem Biol 7, 885-887.

434 Karginov, F.V., Hannon, G.J., 2013. Remodeling of Ago2-mRNA interactions upon cellular stress
435 reflects miRNA complementarity and correlates with altered translation rates. Genes Dev 27,
436 1624-1632.

437 Klann, K., Bojkova, D., Tascher, G., Ciesek, S., Munch, C., Cinatl, J., 2020. Growth Factor
438 Receptor Signaling Inhibition Prevents SARS-CoV-2 Replication. Molecular cell 80, 164-174
439 e164.

440 Kobayashi, K., Hernandez, L.D., Galan, J.E., Janeway, C.A., Jr., Medzhitov, R., Flavell, R.A.,
441 2002. IRAK-M is a negative regulator of Toll-like receptor signaling. Cell 110, 191-202.

442 Lesbirel, S., Wilson, S.A., 2019. The m(6)Amethylase complex and mRNA export. Biochim
443 Biophys Acta Gene Regul Mech 1862, 319-328.

444 Li, N., Hui, H., Bray, B., Gonzalez, G.M., Zeller, M., Anderson, K.G., Knight, R., Smith, D., Wang,
445 Y., Carlin, A.F., Rana, T.M., 2021a. METTL3 regulates viral m6A RNA modification and host cell
446 innate immune responses during SARS-CoV-2 infection. Cell Rep 35, 109091.

447 Li, Y., Renner, D.M., Comar, C.E., Whelan, J.N., Reyes, H.M., Cardenas-Diaz, F.L., Truitt, R.,
448 Tan, L.H., Dong, B., Alysandratos, K.D., Huang, J., Palmer, J.N., Adappa, N.D., Kohanski, M.A.,
449 Kotton, D.N., Silverman, R.H., Yang, W., Morrisey, E.E., Cohen, N.A., Weiss, S.R., 2021b. SARS-
450 CoV-2 induces double-stranded RNA-mediated innate immune responses in respiratory
451 epithelial-derived cells and cardiomyocytes. Proc Natl Acad Sci U S A 118.

452 Liu, J., Cheng, L.G., Li, H.G., 2019. LncRNA SNHG20 promoted the proliferation of glioma cells
453 via sponging miR-4486 to regulate the MDM2-p53 pathway. Eur Rev Med Pharmacol Sci 23,
454 5323-5331.

455 Liu, J., Xu, Y.P., Li, K., Ye, Q., Zhou, H.Y., Sun, H., Li, X., Yu, L., Deng, Y.Q., Li, R.T., Cheng,
456 M.L., He, B., Zhou, J., Li, X.F., Wu, A., Yi, C., Qin, C.F., 2021. The m(6)A methylome of SARS-
457 CoV-2 in host cells. Cell Res 31, 404-414.

458 Liu, J., Yue, Y., Han, D., Wang, X., Fu, Y., Zhang, L., Jia, G., Yu, M., Lu, Z., Deng, X., Dai, Q.,
459 Chen, W., He, C., 2014. A METTL3-METTL14 complex mediates mammalian nuclear RNA N6-
460 adenosine methylation. Nat Chem Biol 10, 93-95.

461 Liu, J., Zhao, Y., Chen, L., Li, R., Ning, Y., Zhu, X., 2022. Role of metformin in functional
462 endometrial hyperplasia and polycystic ovary syndrome involves the regulation of
463 MEG3/miR223/GLUT4 and SNHG20/miR4486/GLUT4 signaling. Mol Med Rep 26.

464 Londres, H.D., Armada, J.J., Martinez, A.H., Abdo Cuza, A.A., Sanchez, Y.H., Rodriguez, A.G.,
465 Figueroa, S.S., Llanez Gregorich, E.M., Torres Lahera, M.L., Peire, F.G., Gonzalez, T.M.,
466 Gonzalez, Y.Z., Ane Kouri, A.L., Palomo, A.G., Concepcion, M.T., Perez, L.M., Luaces-Alvarez,
467 P.L., Iglesias, D.E., Hernandez, D.S., Suzarte, M.R., Ramos, T.C., 2022. Blocking EGFR with
468 nimotuzumab: a novel strategy for COVID-19 treatment. Immunotherapy 14, 521-530.

469 Matsuyama, T., Kubli, S.P., Yoshinaga, S.K., Pfeffer, K., Mak, T.W., 2020. An aberrant STAT
470 pathway is central to COVID-19. Cell Death Differ 27, 3209-3225.

471 McFadden, M.J., Horner, S.M., 2021. N(6)-Methyladenosine Regulates Host Responses to Viral
472 Infection. Trends Biochem Sci 46, 366-377.

473 McFadden, M.J., McIntyre, A.B.R., Mourelatos, H., Abell, N.S., Gokhale, N.S., Ipas, H.,
474 Xhemalce, B., Mason, C.E., Horner, S.M., 2021. Post-transcriptional regulation of antiviral gene
475 expression by N6-methyladenosine. Cell Rep 34, 108798.

476 McIntyre, A.B.R., Gokhale, N.S., Cerchietti, L., Jaffrey, S.R., Horner, S.M., Mason, C.E., 2020.
477 Limits in the detection of m(6)A changes using MeRIP/m(6)A-seq. Sci Rep 10, 6590.

478 Patil, D.P., Pickering, B.F., Jaffrey, S.R., 2018. Reading m(6)A in the Transcriptome: m(6)A-
479 Binding Proteins. Trends Cell Biol 28, 113-127.

480 Roundtree, I.A., Luo, G.Z., Zhang, Z., Wang, X., Zhou, T., Cui, Y., Sha, J., Huang, X., Guerrero,
481 L., Xie, P., He, E., Shen, B., He, C., 2017. YTHDC1 mediates nuclear export of N(6)-
482 methyladenosine methylated mRNAs. Elife 6.

483 Rubio, R.M., Depledge, D.P., Bianco, C., Thompson, L., Mohr, I., 2018. RNA m(6) A modification
484 enzymes shape innate responses to DNA by regulating interferon beta. Genes Dev 32, 1472-
485 1484.

486 Shi, H., Wei, J., He, C., 2019. Where, When, and How: Context-Dependent Functions of RNA
487 Methylation Writers, Readers, and Erasers. Molecular cell 74, 640-650.

488 Tarca, A.L., Draghici, S., Khatri, P., Hassan, S.S., Mittal, P., Kim, J.S., Kim, C.J., Kusanovic, J.P.,
489 Romero, R., 2009. A novel signaling pathway impact analysis. Bioinformatics 25, 75-82.

490 Uhlen, M., Fagerberg, L., Hallstrom, B.M., Lindskog, C., Oksvold, P., Mardinoglu, A., Sivertsson,
491 A., Kampf, C., Sjostedt, E., Asplund, A., Olsson, I., Edlund, K., Lundberg, E., Navani, S.,
492 Szigyarto, C.A., Odeberg, J., Djureinovic, D., Takanen, J.O., Hober, S., Alm, T., Edqvist, P.H.,
493 Berling, H., Tegel, H., Mulder, J., Rockberg, J., Nilsson, P., Schwenk, J.M., Hamsten, M., von
494 Feilitzen, K., Forsberg, M., Persson, L., Johansson, F., Zwahlen, M., von Heijne, G., Nielsen, J.,
495 Ponten, F., 2015. Proteomics. Tissue-based map of the human proteome. Science 347, 1260419.

496 Vagapova, E.R., Lebedev, T.D., Prassolov, V.S., 2021. Viral fibrotic scoring and drug screen
497 based on MAPK activity uncovers EGFR as a key regulator of COVID-19 fibrosis. Sci Rep 11,
498 11234.

499 Venkataraman, T., Frieman, M.B., 2017. The role of epidermal growth factor receptor (EGFR)
500 signaling in SARS coronavirus-induced pulmonary fibrosis. Antiviral Res 143, 142-150.

501 Villarino, A.V., Kanno, Y., O'Shea, J.J., 2017. Mechanisms and consequences of Jak-STAT
502 signaling in the immune system. Nat Immunol 18, 374-384.

503 Wang, X., Lu, Z., Gomez, A., Hon, G.C., Yue, Y., Han, D., Fu, Y., Parisien, M., Dai, Q., Jia, G.,
504 Ren, B., Pan, T., He, C., 2014. N6-methyladenosine-dependent regulation of messenger RNA
505 stability. Nature 505, 117-120.

506 Wang, X., Zhao, B.S., Roundtree, I.A., Lu, Z., Han, D., Ma, H., Weng, X., Chen, K., Shi, H., He,
507 C., 2015. N(6)-methyladenosine Modulates Messenger RNA Translation Efficiency. Cell 161,
508 1388-1399.

509 Warda, A.S., Kretschmer, J., Hackert, P., Lenz, C., Urlaub, H., Hobartner, C., Sloan, K.E.,
510 Bohnsack, M.T., 2017. Human METTL16 is a N(6)-methyladenosine (m(6)A) methyltransferase
511 that targets pre-mRNAs and various non-coding RNAs. EMBO Rep 18, 2004-2014.

512 Williams, G.D., Gokhale, N.S., Horner, S.M., 2019. Regulation of Viral Infection by the RNA
513 Modification N6-Methyladenosine. Annu Rev Virol 6, 235-253.

514 Winkler, R., Gillis, E., Lasman, L., Safra, M., Geula, S., Soyris, C., Nachshon, A., Tai-Schmiedel,
515 J., Friedman, N., Le-Trilling, V.T.K., Trilling, M., Mandelboim, M., Hanna, J.H., Schwartz, S.,
516 Stern-Ginossar, N., 2019. m(6)A modification controls the innate immune response to infection
517 by targeting type I interferons. Nat Immunol 20, 173-182.

518 Zaccara, S., Jaffrey, S.R., 2020. A Unified Model for the Function of YTHDF Proteins in Regulating
519 m(6)A-Modified mRNA. Cell 181, 1582-1595 e1518.

520 Zhang, X., Hao, H., Ma, L., Zhang, Y., Hu, X., Chen, Z., Liu, D., Yuan, J., Hu, Z., Guan, W., 2021.
521 Methyltransferase-like 3 Modulates Severe Acute Respiratory Syndrome Coronavirus-2 RNA N6-
522 Methyladenosine Modification and Replication. mBio 12, e0106721.

523 Zhao, X., Yang, Y., Sun, B.F., Shi, Y., Yang, X., Xiao, W., Hao, Y.J., Ping, X.L., Chen, Y.S., Wang,
524 W.J., Jin, K.X., Wang, X., Huang, C.M., Fu, Y., Ge, X.M., Song, S.H., Jeong, H.S., Yanagisawa,
525 H., Niu, Y., Jia, G.F., Wu, W., Tong, W.M., Okamoto, A., He, C., Rendtlew Danielsen, J.M., Wang,
526 X.J., Yang, Y.G., 2014. FTO-dependent demethylation of N6-methyladenosine regulates mRNA
527 splicing and is required for adipogenesis. Cell Res 24, 1403-1419.

528 Zheng, G., Dahl, J.A., Niu, Y., Fedorcsak, P., Huang, C.M., Li, C.J., Vagbo, C.B., Shi, Y., Wang,
529 W.L., Song, S.H., Lu, Z., Bosmans, R.P., Dai, Q., Hao, Y.J., Yang, X., Zhao, W.M., Tong, W.M.,
530 Wang, X.J., Bogdan, F., Furu, K., Fu, Y., Jia, G., Zhao, X., Liu, J., Krokan, H.E., Klungland, A.,
531 Yang, Y.G., He, C., 2013. ALKBH5 is a mammalian RNA demethylase that impacts RNA
532 metabolism and mouse fertility. Molecular cell 49, 18-29.

533 Zheng, Q., Hou, J., Zhou, Y., Li, Z., Cao, X., 2017. The RNA helicase DDX46 inhibits innate
534 immunity by entrapping m(6)A-demethylated antiviral transcripts in the nucleus. Nat Immunol 18,
535 1094-1103.

536 Zhou, C., Chen, L., Chen, R., Xu, F., Huang, Z., Huang, R., Wang, W., Xu, Q., 2022. miR-4486
537 enhances cisplatin sensitivity of gastric cancer cells by restraining the JAK3/STAT3 signalling
538 pathway. J Chemother 34, 35-44.

539 Zotti, T., Vito, P., Stilo, R., 2012. The seventh ring: exploring TRAF7 functions. J Cell Physiol 227,
540 1280-1284.

541

Figures 1-5 and legends

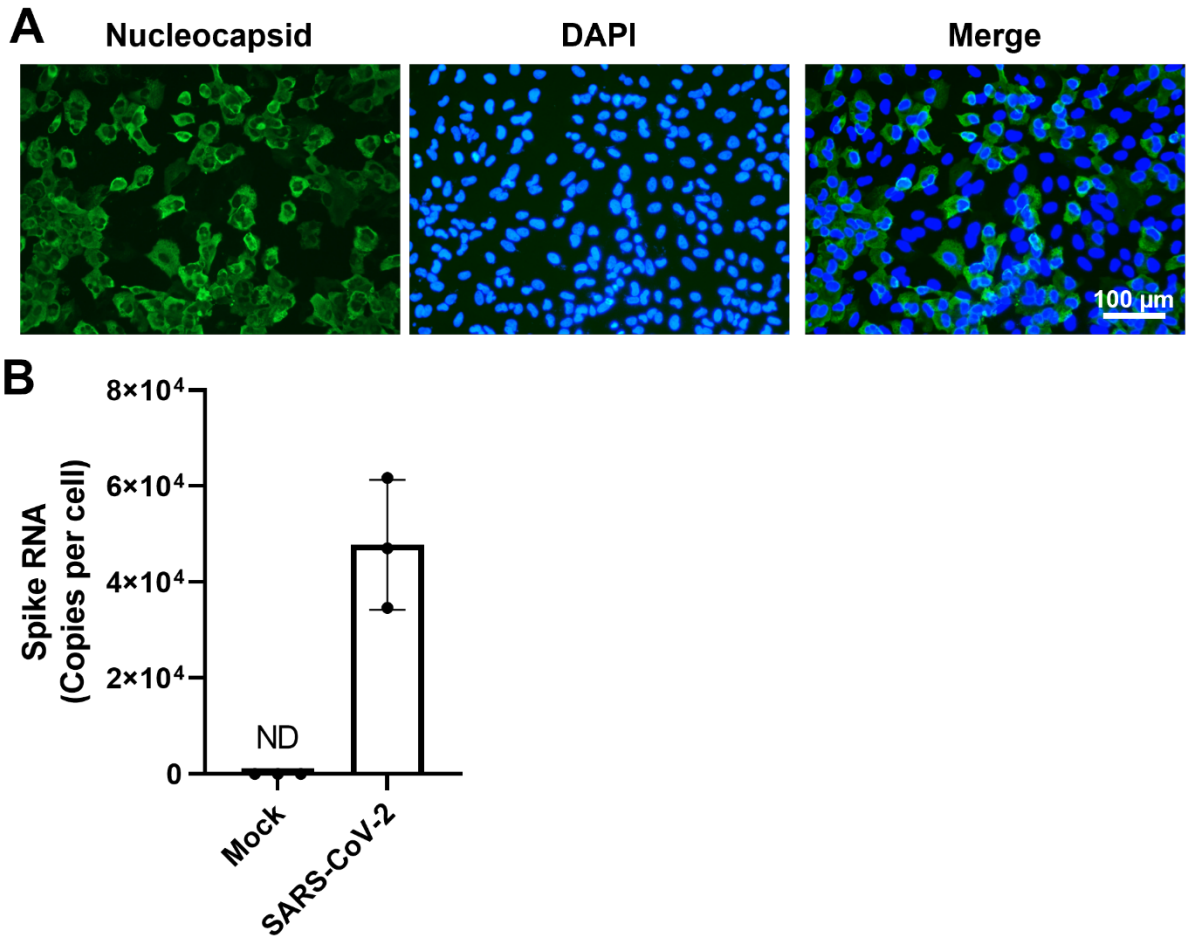

Fig. 1. SARS-CoV-2 infection of A549-hACE2 cells. A549-hACE2 cells were infected with SARS-CoV-2 (strain USA-WA1/2020) at an MOI of 1 for 24 hours. (**A**) Immunofluorescent staining was performed to visualize infected cells by the presence of SARS-CoV-2 nucleocapsid (green). Nuclei of cells are stained with DAPI (blue). (**B**) SARS-CoV-2 spike RNA in infected cells (N=3, biological triplicate) was quantified by RT-qPCR. ND: not detected.

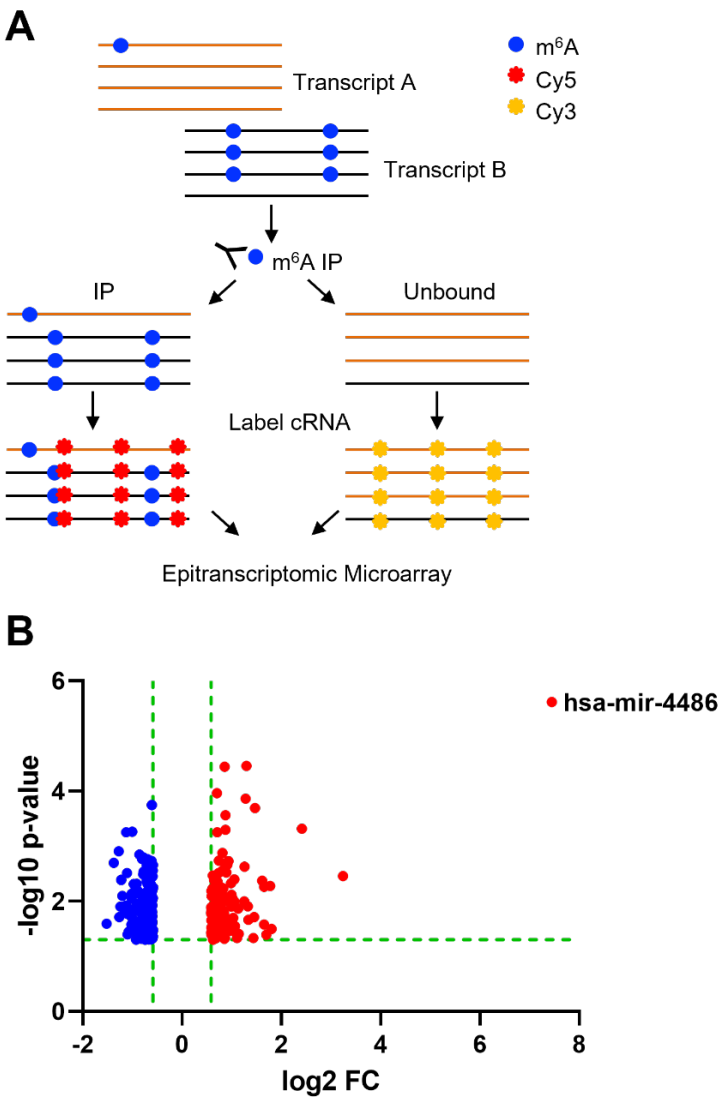

Fig. 2. Epitranscriptomic m^{6}A microarray of SARS-CoV-2-infected A549-hACE2 cells. (**A**) Schematic overview of the method. Total cellular RNA from each sample (SARS-CoV-2-infected and mock-infected controls, biological triplicate, N=3 each group) was used for immunoprecipitation using an m^{6}A-specific antibody. Methylated and unmethylated RNA fractions were fluorescently labeled (Cy3 or Cy5) prior to array hybridization (refer to Materials and Methods for details). (**B**) Volcano plot of transcripts containing higher (red) and lower (blue) levels of m^{6}A modification in infected cells compared to mock-infected control cells. The miRNA precursor (hsa-mir-4486) with the most significant m^{6}A change is labeled.

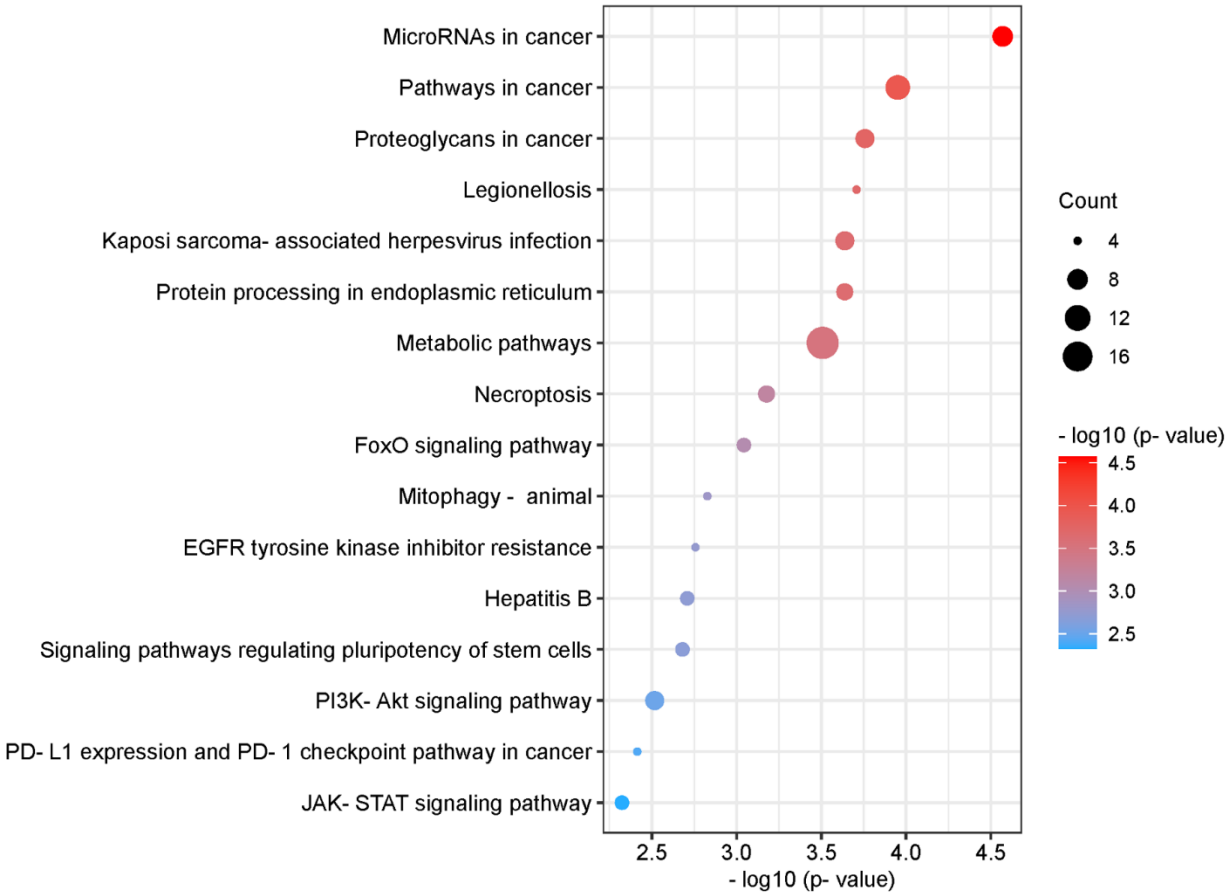

Fig. 3. Pathway analysis of differentially methylated mRNAs. List of pathways associated with differentially methylated mRNAs with the highest combined significance (pORA and pAcc ≤ 0.005). Significance is indicated on the x-axis and by sphere color. The size of the sphere corresponds to the number of differentially methylated mRNAs associated with each pathway (count). Bubble plot was created using https://www.bioinformatics.com.cn/en, a free online platform for data analysis and visualization.

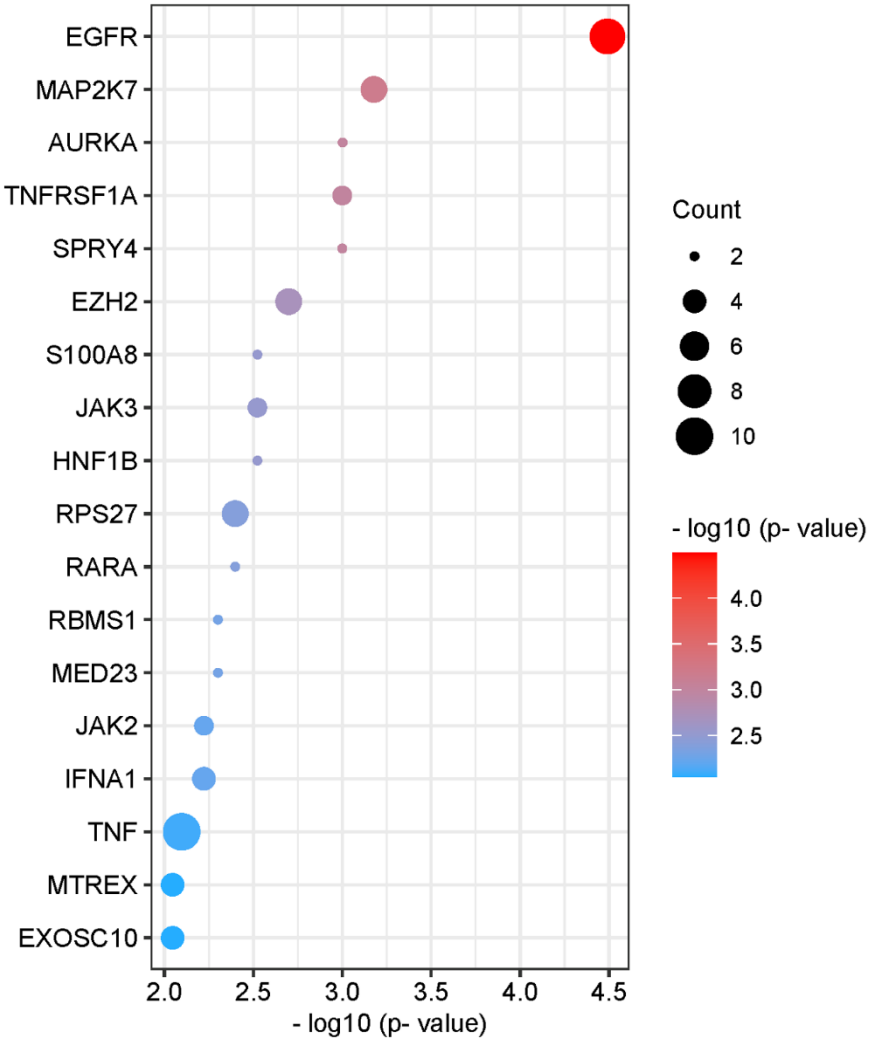

Fig. 4. Upstream regulators of differentially methylated mRNAs. List of upstream regulators associated with differentially methylated mRNAs with the highest significance ($p \leq 0.01$). Significance is indicated on the x-axis and by sphere color. The size of the sphere corresponds to the number of differentially methylated mRNAs associated with each pathway (count). Bubble plot was created using https://www.bioinformatics.com.cn/en, a free online platform for data analysis and visualization.

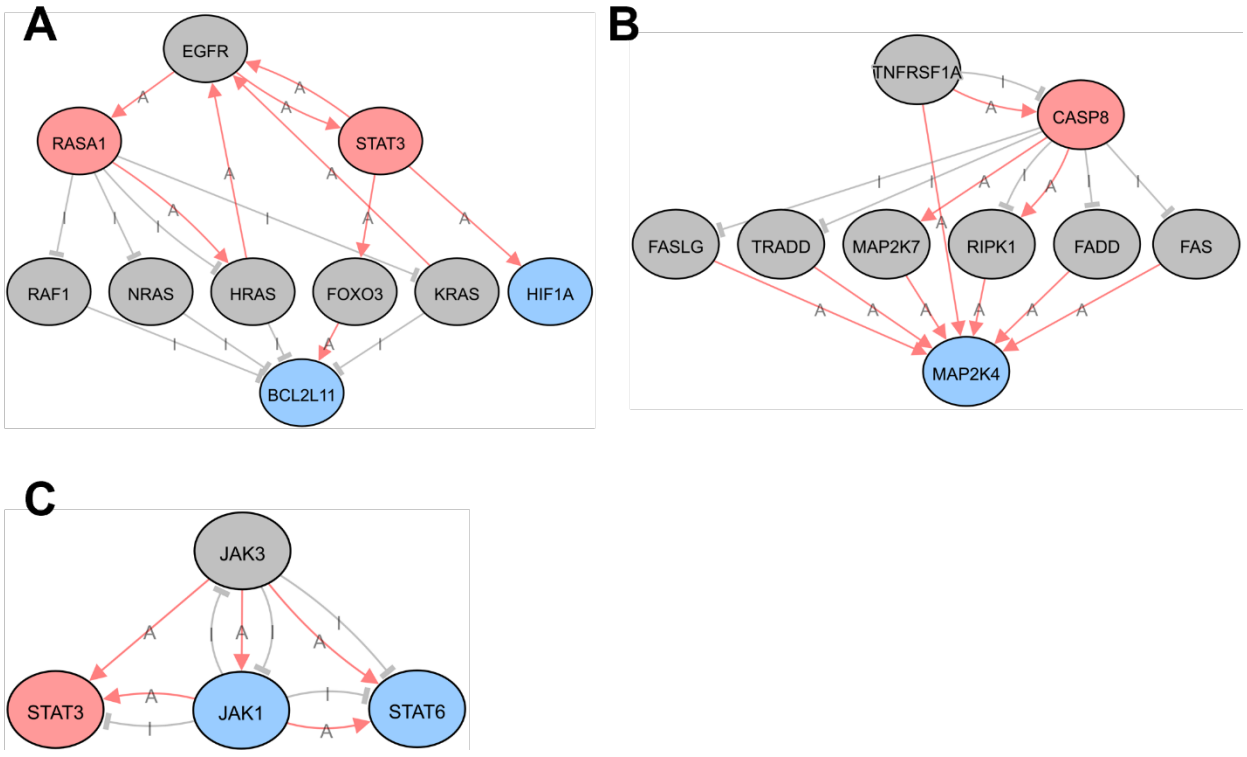

Fig. 5. Predicted upstream regulator networks. Network map of selected upstream regulators of differentially methylated mRNA transcripts. Upstream regulators are **(A)** EGFR, **(B)** TNFRSF1A, and **(C)** JAK3. Colors represent the change in m^6A modification of indicated transcripts in response to SARS-CoV-2 infection in human lung epithelial cells. Gray circles: no change; pink circles: hypermethylated; blue circles: hypomethylated. Lines indicate known functional interactions between pathway nodes. Pink arrows: activation (A); gray bars: inhibition (I). Images were obtained using iPathwayGuide from AdvaitaBio.

610 **Tables**

611 **Table 1.** Summary of differentially modified transcripts by type in SARS-CoV-2-infected A549-
612 hACE2 cells vs. mock-infected control cells.

613

Transcript Type	Hypo m^6A	Hyper m^6A	Total	Numbers of Probes
mRNA	160	89	249	44,122
lncRNA	24	22	46	12,496
sncRNA	2	8	10	3,813

614 Fold change ≥ 1.5 and p ≤ 0.05

615 **Table 2.** Selected differentially m^{6}A-modified transcripts in SARS-CoV-2-infected A549-hACE2
616 cells vs. mock-infected control cells by m^{6}A quantity.

Transcript Type	Transcript ID	Gene Symbol	Log2 Fold Change	p-value
mRNA	ENST00000250457	EGLN3	0.8595436	3.609E-05
mRNA	HBMT00001402195	CATG00000101027.1	1.4687341	0.0002032
mRNA	ENST00000540159	BNIP3	0.8732292	0.0002728
mRNA	ENST00000325885	ASB4	2.4125726	0.0004796
mRNA	ENST00000618819	PTPN9	0.8113196	0.0013265
mRNA	NM_001330464	ATL2	0.9303607	0.0018649
mRNA	ENST00000357077	ANK2	0.8673231	0.0021318
mRNA	ENST00000422053	TRIB3	0.9064073	0.0021784
mRNA	ENST00000528331	SYBU	1.255638	0.0023711
mRNA	ENST00000311450	PLAC8L1	0.8936838	0.0029927
mRNA	ENST00000382181	RBCK1	0.7350803	0.0030862
mRNA	ENST00000248071	KLF2	0.6192452	0.0034099
mRNA	ENST00000374448	MUSK	3.2415767	0.0034892
mRNA	ENST00000376468	NPPB	1.0536428	0.0040088
mRNA	ENST00000371445	DMRTB1	0.6458079	0.0041402
mRNA	ENST00000644112	TIMM8A	-0.6091437	0.0001784
mRNA	ENST00000360948	NTRK3	-1.0030983	0.0005479
mRNA	ENST00000629765	NTRK3	-1.1272045	0.0005579
mRNA	ENST00000394480	NTRK3	-1.2754039	0.0012382
mRNA	ENST00000417456	RP11-244H3.5	-0.8596983	0.0014264
mRNA	ENST00000619416	KIAA0586	-0.7813802	0.0015997
mRNA	ENST00000539097	HIF1A	-0.8053586	0.0017167
mRNA	ENST00000451528	ST8SIA4	-0.6902188	0.0017212
mRNA	NM_001320134	NTRK3	-0.61504	0.0018528
mRNA	ENST00000378133	PCDHA1	-0.5856729	0.0022007
mRNA	ENST00000333896	SPTBN1	-0.7070035	0.002238
mRNA	ENST00000368581	RSPH4A	-0.6288855	0.0026367
mRNA	ENST00000394332	RPL23	-0.6408456	0.0026379
mRNA	ENST00000357496	QRICH1	-0.593256	0.0027733
mRNA	ENST00000537259	SLC24A1	-0.7748985	0.0028879
mRNA	MICT00000118072	CATG00000023300.1	-0.6383486	0.0029291
mRNA	ENST00000644112	TIMM8A	-0.6091437	0.0001784
mRNA	ENST00000360948	NTRK3	-1.0030983	0.0005479
lncRNA	NR_148507	AC010982.1	1.2975579	3.476E-05
lncRNA	ENST00000477817	PKP1	0.7016014	0.0001088
lncRNA	NR_152836	PSORS1C3	1.2784829	0.0001375
lncRNA	ENST00000579368	RP11-674N23.1	0.8775907	0.0005063
lncRNA	ENST00000592680	AC007773.2	0.7066193	0.0005585
lncRNA	ENST00000436551	AC104654.2	-1.3765495	0.0020037
lncRNA	NR_136184	CENPO	-0.7059265	0.0026148
lncRNA	ENST00000503936	TTC33	-0.6501871	0.0027399
lncRNA	ENST00000422847	RP11-40F6.2	-0.6267391	0.0050007
pre-miRNA	MI0001446	hsa-mir-4486	7.4490146	2.413E-06

617 $p \leq 0.005$

618 **Table 3.** Selected differentially m^{6}A-modified transcripts in SARS-CoV-2-infected A549-hACE2
619 cells vs. mock-infected control cells by % modified.

620

Transcript Type	Transcript ID	Gene Symbol	% Mock	% SARS-CoV-2
mRNA	ENST00000374448	MUSK	30%	69%
mRNA	ENST00000371968	LHFPL1	33%	43%
mRNA	ENST00000264657	STAT3	27%	34%
mRNA	ENST00000528331	SYBU	40%	53%
mRNA	ENST00000360375	LRRCC1	40%	23%
mRNA	ENST00000361987	CNTF	91%	81%
mRNA	ENST00000216513	SIX4	93%	82%
mRNA	ENST00000367512	EDEM3	83%	69%
mRNA	ENST00000522232	CTB-83D3.1	72%	34%
mRNA	ENST00000361028	ZSCAN12	80%	54%
lncRNA	NR_145484	ARHGAP32	91%	74%
lncRNA	NR_015352	CECR7	65%	32%
pre-miRNA	MI0001446	hsa-mir-4486	44%	73%

621 $p \leq 0.005$

Supplementary Tables (two separate Excel files)

Table S1: All differentially m^{6}a-modified transcripts in SARS-CoV-2-infected A549-hACE2 cells vs. mock-infected control cells.

Table S2: All pathways associated with at least one differentially methylated mRNA in SARS-CoV-2-infected A549-hACE2 cell vs. mock-infected control cells.